Published in final edited form as:

J Magn Reson Imaging. 2009 May ; 29(5): 1071–1079. doi:10.1002/jmri.21737.

MRI Methods for Evaluating the Effects of Tyrosine Kinase Inhibitor Administration Used to Enhance Chemotherapy Efficiency in a Breast Tumor Xenograft Model

S.O. Aliu, BS[1,2,*], **L.J. Wilmes, PhD**[1], **M.M. Moasser, MD**[3], **B.C. Hann, MD, PhD**[4], **K.-L. Li, PhD**[1], **D. Wang, BS**[4], and **N.M. Hylton, PhD**[1,2]

[1]Department of Radiology and Biomedical Imaging, University of California at San Francisco, San Francisco, California

[2]Joint Graduate Group in Bioengineering, University of California at Berkeley and San Francisco, California

[3]Department of Medicine, University of California at San Francisco, San Francisco, California

[4]Helen Diller Family Comprehensive Cancer Center, University of California at San Francisco, San Francisco, California

Abstract

Purpose—To evaluate whether quantitative MRI parameters are sensitive to the effects of the tyrosine kinase inhibitor gefitinib and can discriminate between two different treatment protocols.

Materials and Methods—Untreated mice with BT474 breast tumor xenografts were characterized in a preliminary study. Subsequently, tumor volume, apparent diffusion coefficient (ADC), transendothelial permeability (K^{ps}), and fractional plasma volume (fPV) were measured in three groups of mice receiving: 1) control vehicle for 10 days, or gefitinib as 2) a single daily dose for 10 days or 3) a 2-day pulsed dose.

Results—Gefitinib treatment resulted in significant tumor growth inhibition (pulsed: 439 ± 93; daily: 404 ± 53; control: 891 ± 174 mm^3, $P < 0.050$) and lower cell density (pulsed: 0.15 ± 0.01, daily: 0.17 ± 0.01, control: 0.24 ± 0.01, $P < 0.050$) after 9 days. Tumor ADC increased in treated groups but decreased in controls ($P > 0.050$). Tumor K^{ps} decreased with pulsed treatment but rebounded afterwards and increased with daily treatment ($P > 0.050$). Tumor fPV increased in both treated groups, decreasing afterwards with pulsed treatment ($P > 0.050$).

Conclusion—Quantitative MRI can provide a sensitive measure of gefitinib-induced tumor changes, potentially distinguish between treatment regimens, and may be useful for determining optimal treatment scheduling for enhancing chemotherapy delivery.

Keywords

chemotherapy; dynamic contrast enhanced; diffusion weighted imaging; gefitinib; tyrosine kinase inhibitor; xenograft tumor model

[*]Address reprint requests to: Sheye O. Aliu, UCSF Department of Radiology, Box 0946, San Francisco CA, 94107. sheye.aliu@radiology.ucsf.edu.

A PROMISING APPROACH to improving antitumor efficacy in cancer treatment involves the combination of targeted agents aimed at inhibiting signal transduction in tumors with cytotoxic drugs. An advantage to this approach is that signaling pathways and associated receptors implicated in different cancer types can be specifically targeted. The human growth factor receptor (HER) family of tyrosine kinases (TKs) plays an important role in cell differentiation, proliferation, migration, and survival (1). HER TKs have been implicated in breast cancer (2) and mediate some of the angiogenic properties of cancer cells (3,4). Dysregulation of HER TKs has been shown to promote the development and growth of cancer (1). This makes HER TKs an attractive target for the design of antitumor targeting agents.

Gefitinib (Iressa), an HER family tyrosine kinase inhibitor (TKI), has demonstrated antitumor activity in HER family overexpressing breast tumor cells in vitro and in vivo (5,6). Preclinical studies have shown enhanced efficacy from the combined administration of gefitinib with chemotherapy (7,8). However, this effect was moderate and recent evidence suggests that the ability of gefitinib to suppress survival signaling might be transient, requiring much higher doses to effectively suppress HER family survival signaling (9). High daily doses of HER TKIs are impractical due to their dose-limiting toxicities. However, when used as chemosensitizers, HER TKIs can be administered for short periods in much higher doses immediately prior to chemotherapy and can potentially serve to prime tumor microenvironments for better delivery of chemotherapeutic agents. Optimal priming of the tumor microenvironment will likely depend on precise timing of HER TKI administration relative to chemotherapy. Measurement methods that are sensitive to the effects of HER TKIs and can be used for in vivo monitoring are needed.

MRI methods have been used to detect changes induced by other targeting agents, notably those directed toward the vascular endothelial growth factor (VEGF) (10), but few studies have applied MRI to study the effects of HER family targeting agents. The present study assessed the ability of multiple MRI parameters, including tumor volume, apparent diffusion coefficient (ADC), transendothelial permeability (K^{ps}), and fractional plasma volume (fPV) to detect gefitinib induced changes in a breast tumor xenograft model.

The ADC, obtained from diffusion-weighted MRI, is a noninvasive imaging technique that measures the mobility of water in tissues. Diffusion in MRI is generally observed through the introduction of a pair of bipolar motion sensitizing gradient pulses (11). Studies have shown that the ADC is inversely correlated with tissue cellularity (12,13), reflecting greater restriction to motion in denser tissue. In recent years the ADC has emerged as a potential surrogate indicator of tumor response to therapy (14–16) and has been used to differentiate malignant tumors from benign lesions and normal tissue (17–20).

Dynamic contrast-enhanced (DCE)-MRI is a technique for evaluating the physiology of microcirculation. It entails serial acquisition of MR images before, during, and after intravenous injection of contrast media into tissues of interest. By fitting DCE-MRI data acquired using macromolecular contrast media such as albumin-$(GdDTPA)_{30}$ to an appropriate pharmacokinetic model, it is possible to extract quantitative physiologic

parameters that describe microvascular wall permeability (K^{ps}) and the fPV. Numerous studies have used DCE-MRI to assess vascular changes associated with response to antiangiogenic therapy (21–24). Several studies have demonstrated decreased K^{ps} in response to effective antiangiogenic therapy, which is generally attributed to less leaky vessels. The fPV has also been used as a surrogate marker of tumor angiogenesis.

The aims of the present study were to evaluate the ability of MRI parameters to detect the effects of gefitinib administered as a potential means of improving chemotherapy administration and to evaluate whether MRI parameters can differentiate between two different gefitinib treatment regimens.

Materials and Methods

Tumor Model

Immune deficient female mice (*Nu/nu*; age 7–8 weeks; Taconic, Germantown, NY) were implanted subcutaneously with 17β estradiol pellets (0.72 mg/pellet; Innovative Research, Sarasota, FL) 24–48 hours prior to tumor cell injection. Human BT474, HER2-neu overexpressing breast cancer cells optimized for growth in vivo were implanted subcutaneously into the axillary flank (1×10^7 cells/injection). Tumors were allowed to grow to ≈200–400 mm^3 (typically 2 weeks after cell injection) prior to imaging or treatment. All animal usage was approved by the institutional Animal Care Committee.

In Vivo MRI Studies

Natural History—To establish the natural history of MRI parameters during the growth of BT474 tumors, a cohort of untreated mice ($n = 8$) were imaged beginning 2 weeks after tumor cell injection, at ≈2-day intervals over a 2-week period: baseline, day 2, day 4, day 7, day 9, day 11, and day 14. Diffusion-, T_1-, and T_2-weighted images were acquired at each timepoint in all mice.

Gefitinib Treatment Study—For the treatment study, tumor-bearing mice were treated with gefitinib according to three arms: daily dose ($n = 6$), pulsed dose ($n = 6$), and controls ($n = 5$). In the daily treatment arm, mice were treated daily with gefitinib at the maximum tolerated daily dose of 150 mg/kg orally (po) for 10 days. In the pulsed treatment arm, mice were treated for 2 days (days 2 and 3) with gefitinib at the maximum tolerated dose of 1000 mg/kg po. Control mice were treated daily with vehicle carrier for 10 days. All treatments were administered by oral gavage and mice in all three arms were imaged at baseline, day 4, and day 9. In addition to diffusion-, T_1-, and T_2-weighted images, DCE images were acquired at each timepoint. Figure 1 illustrates the imaging and dosing schedule for the gefitinib treatment study.

MRI

MRI was performed on a whole-body 1.5T GE Signa scanner (GE Healthcare, Milwaukee, WI) using a wrist coil (Medical Advances, Milwaukee, WI) and customized animal holder. Mice were imaged in pairs and were anesthetized by inhalation with 1.5% isoflurane administered via an MR-compatible mobile inhalation anesthesia system (Vet Equip,

Pleasanton, CA). A 3D fast gradient recalled echo (FGRE) sequence was used to rapidly and reproducibly position mice.

Diffusion-weighted images were acquired using a diffusion-sensitized single-shot fast spin echo sequence (TR = 9899 msec, effective TE = 69 msec, field of view (FOV) = 100 × 100 mm, slice thickness = 3 mm, imaging matrix = 256 × 256). Ten axial diffusion-weighted slices centered around the tumor were acquired. Diffusion weighting was achieved with a gradient duration δ = 17.6 msec, gradient interval Δ = 22.8 msec, gradient strength G_D = 39.6 mT/m, and the *b*-value was calculated according to:

$$b=\gamma^2 G_D^2 \delta^2 \left(\Delta - \frac{\delta}{3}\right)$$

where γ is the gyromagnetic ratio of the proton. Weighting factors (*b*-values) of *b* = 0 and *b* = 603 s/mm^2 were applied.

T_1-weighted images were acquired using a variable flip angle 3D spoiled gradient echo sequence (TR = 27 msec, TE = 8 msec, flip angle = 40°, 20°, 8°, FOV = 100 × 100 mm, slice thickness =1 mm, imaging matrix = 256 × 256 × 28).

T_2-weighted images were acquired using a fast spin echo sequence (TR = 5500 msec, TE = 81 msec, FOV = 100 × 100 mm, slice thickness = 1.5 mm, imaging matrix = 256 × 256).

Contrast-enhanced imaging was performed using a coronal T_1-weighted 3D FGRE sequence (TR = 9 msec, TE = 4ms, FOV = 100 × 100 mm, slice thickness = 1 mm, imaging matrix = 256 × 256 × 28, acquisition time = 63 sec). Axial images were acquired for tumor localization and five precontrast scans were acquired prior to injecting 0.03 mmol/kg albumin-$(GdDTPA)_{30}$ (Center for Pharmaceutical and Molecular Imaging at UCSF, San Francisco, CA) via the tail vein (25). This was followed by 40 minutes of postcontrast imaging.

Image Analysis

MRI tumor volume was approximated on noncontrast enhanced 3D T_1-weighted images by manually delineating tumor boundary regions of interest (ROIs) sequentially on all tumor-appearing slices and summing the volumes. A single operator delineated all ROIs to ensure consistency. ADC maps were generated on a pixel-by-pixel basis from diffusion-weighted images as described previously (26). T_1 maps were generated from T_1-weighted images acquired at the three flip angles, 40°, 20°, and 8°. A fitting routine implemented in IDL (v. 6.1; Research Systems, Boulder, CO) was used to generate T_1 maps.

To interrogate potential effects of tumor necrosis on measurements, necrotic regions—typically presenting as hyperintense regions on T_2-weighted images—were isolated using a semiautomated clustering technique (27,28) implemented in MatLab (R2006a; MathWorks, Natick, MA). Clusters were generated by considering T_2-weighted signal intensities in the entire tumor on a pixel-by-pixel basis and assigning pixels to clusters to minimize

intracluster variance. Generated clusters were subsequently categorized as potentially necrotic based on visual inspection. Such potentially necrotic clusters were then classified as necrotic if pixel signal intensities were beyond three standard deviations from mean tumor T_2-weighted signal intensity. Five clusters were imposed to oversample the number of tumor components and empirically determined to provide the best compromise between maximizing tissue differentiation and minimizing computation time. Pixels on ADC maps corresponding to necrotic clusters on T_2-weighted images were excluded from ADC analysis. Figure 2 illustrates the segmentation of necrotic regions.

Quantitative analysis of T_1-weighted, albumin-$(Gd\text{-}DTPA)_{30}$ enhanced images was performed using a two-compartment unidirectional pharmacokinetic model incorporating precontrast tissue T_1 values to estimate K^{ps} and fPV from the relationship:

$$C_t(t) = K^{ps} \int_0^t C_p(t')\,dt' + fPV \cdot C_p(t)$$

where C_t and C_p are the concentrations of contrast media in tissue and plasma, respectively, as described previously (29–31). Tumor boundaries were assigned manually in the DCE-MRI images. K^{ps} and fPV maps were estimated on a voxel-by-voxel basis for ROIs encompassing the whole tumor. Individual vascular input functions were determined from enhancing voxels in the abdominal aorta of each mouse and were assumed to decay monoexponentially.

Statistics

A one-way repeated-measures analysis of variance (ANOVA) design was used to establish significant differences over time in the natural history study. A two-way repeated measures ANOVA was used to establish differences in MRI parameters (mean tumor ADC, volume, K^{ps}, and fPV) between the treatment groups (pulsed, daily, control) over time (baseline, day 4, day 9) in the gefitinib treatment study. Differences in cell density indices on hematoxylin and eosin (H&E) slides and apoptotic indices on caspase-3 slides, between the treatment groups, were established using a one-way ANOVA design. Tukey's Honestly Significant Difference test was used for post-hoc comparisons in all ANOVA designs. JMP (v. 6; SAS, Cary, NC) was used for all statistics.

Histology and Immunohistochemistry

Mice in the gefitinib treatment study were euthanized immediately following imaging on day 9 and tumor tissues were harvested for histology and immunohistochemistry. Tumors were sectioned along the plane corresponding to DCE and diffusion-weighted image acquisition. Tumor tissues were processed, embedded in paraffin, and sectioned at 5 μm thickness. Consecutive slices were stained with H&E to probe differences in cell density between groups and with rabbit anti-cleaved caspase-3 polyclonal antibody, 1:200 dilution (Cell Signaling Technology, Beverly, MA) to assess potential apoptotic effects and any differences between groups. H&E tissue slides were analyzed on a Nikon microscope (Eclipse TE-2000E; Nikon, Tokyo, Japan). Two to three representative fields from

nonnecrotic regions were chosen from each slide. The microscope manufacturer's software (NIS-Elements AR 2.30) was used to generate a cell density index as the ratio of the area occupied by cells within a field to the total field area. Indices were then averaged for each of the three experimental groups in the gefitinib treatment study. Caspase-3 slides were analyzed on a Nikon microscope (Eclipse TS 100-F; Nikon). A 10 × 10 mm reticule (at magnification 40×) served as the field. An apoptotic index was computed as the ratio of apoptosis stained cells to the total number of cells in the field. This ratio was averaged across slides for each of the three experimental groups in the gefitinib treatment study.

Results

Natural History

MRI mean tumor volume increased exponentially (144 exp(0.25×) mm^3, $R^2 = 0.93$) over the course of the 14-day natural history study (M ± SEM: 187 ± 37, 202 ± 29, 353 ± 52, 370 ± 52, 620 ± 126, 561 ± 99, 758 ± 127 mm^3). There were significant differences ($F(6,47) = 6.27$, $P < 0.0001$) in mean tumor volume over time. Specifically, mean tumor volumes at day 9, day 11, and day 14 were significantly different from mean tumor volumes at baseline ($P < 0.050$). Mean tumor ADC remained relatively uniform over the course of the natural history study (M ± SEM: 1151 ± 28, 1041 ± 66, 1121 ± 59, 1020 ± 74, 1155 ± 70, 1078 ± 56, 1090 ± 55 mm^2/s). Mean tumor T_1 values stabilized after a slight decrease from baseline to day 2 (M ± SEM: 1246 ± 74, 1168 ± 11, 1102 ± 59, 1152 ± 26, 1093 ± 51, 1125 ± 44, 1141 ± 32). Figure 4 displays results in the natural history study.

Gefitinib Treatment Study

Trends in mean tumor volume, ADC, and T_1 observed in the control group of the gefitinib treatment study were consistent with trends observed in untreated mice in the natural history study. Figure 3 displays representative diffusion- and T_1-weighted images and corresponding maps.

Mean tumor volumes increased between baseline and day 9 in all three experimental groups but the two gefitinib-treated groups increased at a slower rate relative to the control group. There was a significant main effect of treatment ($F(2,14.03) = 7.90$, $P = 0.0050$) and time ($F(2,19.56) = 34.69$, $P < 0.0001$) on mean tumor volumes. There was also an interaction effect of treatment and time ($F(4,18.92) = 8.22$, $P = 0.0005$). Post-hoc comparisons revealed that mean tumor volumes in all groups were not significantly different at baseline (M ± SEM; pulsed: 361 ± 25; daily: 244 ± 22; control: 288 ± 30 mm^3, $P > 0.050$) but both gefitinib-treated groups were significantly different from the control group at day 9 (M ± SEM; pulsed: 439 ± 93; daily: 404 ± 53; control: 891 ± 174 mm^3, $P < 0.050$). There was a transient decrease in mean tumor volume observed in the pulsed dose group between baseline and day 4 but this trend was not statistically significant. Figure 5 illustrates all significant differences in mean tumor volume between and within groups.

As a general trend, mean tumor ADC increased in both gefitinib-treated groups between baseline and day 9 (M ± SEM; pulsed: 1034 ± 24, 1141 ± 40, 1212 ± 89; daily:1056 ± 56, 1077 ± 50, 1159 ± 53 mm^2/s) but remained relatively unchanged in the control group from

baseline today 9 (M ± SEM;1198 ±45, 1152 ± 95, 1137 ± 71 mm^2/s). However, there was no statistically significant effect of treatment or time on mean tumor ADC. Figure 5 displays mean tumor ADC trends in the gefitinib treatment study.

Mean tumor K^{ps} decreased from baseline to day 4 with a rebound at day 9 in the pulsed dose group (M ± SEM; 0.0647 ± 0.0215, 0.035 ± 0.0094, 0.0739 ± 0.0048 mL/100g/min), increased from baseline to day 9 in the daily dose group (M ± SEM; 0.0486 ± 0.0054, 0.0586 ± 0.0198, 0.0646 ± 0.0257 mL/100g/min) and decreased from baseline to day 9 in the control group (M ± SEM; 0.0734 ± 0.0064, 0.0652 ± 0.0088, 0.0583 ± 0.0140 mL/100g/min). However, there were no statistical differences between or within the groups. Figure 5 displays mean tumor K^{ps} trends.

Mean tumor fPV increased from baseline to day 4 before decreasing from day 4 to day 9 in the pulsed dose group (M ± SEM; 0.0250 ± 0.0014, 0.0323 ± 0.0026, 0.0223 ± 0.0016), increased from baseline to day 9 in the daily dose group (M ± SEM; 0.0184 ± 0.0030, 0.0271 ± 0.0045, 0.0325 ± 0.0051), and remained relatively uniform from baseline to day 9 in the control group (M ± SEM; 0.0187 ± 0.0026, 0.0212 ± 0.0044, 0.0172 ± 0.0006). There was a trend toward an effect of treatment ($F(2,13.34) = 3.71$, $P = 0.0523$) and a significant main effect of time ($F(2,24.94) = 3.71$, $P = 0.0388$) but no statistically significant interaction between treatment and time on mean tumor fPV. Figure 5 displays mean tumor fPV results.

Histological evaluation of tumors in the natural history study and in the gefitinib treatment study revealed noticeable central necrosis, and in some cases peripheral necrosis. There was a significant effect of treatment ($F(2,10) = 17.86$, $P < 0.0005$) on cell densities computed from H&E slides. Gefitinib-treated groups were significantly less dense than the control group (M ± SEM; pulsed: 0.15 ± 0.01; daily: 0.17 ± 0.01; control: 0.24 ± 0.01, $P < 0.050$) but were not significantly different from each other. Qualitatively, the gefitinib-treated groups were also observed to exhibit greater internuclear spacing relative to the control group. There was no significant effect of treatment on apoptotic indices computed from caspase-3 slides. Table 1 summarizes cell density indices, apoptotic indices, and differences observed in all groups of the gefitinib treatment study. Figures 6 and 7 respectively display representative H&E and caspase-3 stains for all groups in the gefitinib treatment study.

Discussion

To our knowledge, the present study is the first to characterize the untreated BT474 human breast tumor model using MRI parameters as we have reported in the natural history measurements of mean tumor volume, ADC, and T_1. We observed that the mean tumor ADC remained relatively constant over the course of the 14-day natural history study. The ADC is sensitive to differences in tissue cellularity and microstructure. Thus, other factors held constant, it might be expected that increasing cellularity—anticipated by the lack of any intervention in the natural history and supported by exponential growth in mean tumor volume—would induce decreasing water mobility and consequently decreasing ADC values. One explanation for this seeming discrepancy is tissue necrosis; necrotic regions by definition are characterized by lower cellularity, favoring greater water mobility. Although

we made efforts to isolate necrotic pixels from ADC analysis, there may be residual effects of necrotic pixels that could moderately inflate reported ADC values.

In the natural history study, we observed that mean tumor T_1 values remained relatively constant after a slight decrease from baseline to day 2. A similar trend was observed in the control group of the gefitinib treatment study. Precontrast tumor T_1 is a fundamental variable in the pharmacokinetic modeling of DCE-MRI data and our characterization of the T_1 time course in the BT474 xenograft tumor model can potentially serve to inform the analysis of future DCE-MRI studies using the BT474 xenograft tumor model.

Mean tumor volumes distinguished the gefitinib treated groups from the control group; tumor growth was significantly inhibited in both gefitinib-treated groups relative to the control group, suggesting an effect due to gefitinib administration. Mean tumor volumes did not distinguish the gefitinib treatment groups from each other but there was a small reduction in mean tumor volume uniquely observed in the pulsed dose group. This trend is consistent with studies by Moasser et al (32) and Solit et al (33), where they report that pulsatile gefitinib treatment yields greater mean tumor regression and a higher percentage of complete responses than other schedules. Of note, the studies by Moasser et al and Solit et al followed gefitinib with paclitaxel—a cytotoxic agent—whereas the present study examined gefitinib alone and not in concert with any cytotoxic agents.

The gefitinib treatment study revealed a trend of increasing mean tumor ADC in the gefitinib-treated groups, while mean tumor ADC decreased slightly in the control group. Microscopic analysis of H&E slides revealed that both gefitinib-treated groups demonstrated significantly less cell density relative to the control group. The ADC has been demonstrated to correlate inversely with tumor cellularity (12,18,34). Our finding of increasing mean tumor ADC and less cell density in the gefitinib-treated groups is in agreement with studies by other investigators (14–17,20) reporting higher ADC and lower cellularity in treated tumors.

DCE-MRI parameters revealed some unexpected but interesting findings. Mean tumor transendothelial permeability, K^{ps}, was unable to statistically distinguish the treatment groups but observed trends revealed an initial reduction in the pulsed dose group followed by a rebound, an increase over time in the daily dose group, and a slight reduction over time in controls. K^{ps} is a measure of the transfer between the vascular and interstitial spaces. Multiple studies, including studies evaluating VEGF-targeted therapies, have reported reduced K^{ps} in response to effective antiangiogenic therapy (10,35–38). Such a reduction in K^{ps} is thought to reflect a reduction in the leakiness of microvessels. Gefitinib belongs to a class of inhibitors that are capable of targeting HER TKs, which are implicated in endothelial cell signaling and may have antiangiogenic activity (39). The trend toward an initial reduction in K^{ps} observed in the pulsed dose group is consistent with results from studies evaluating VEGF-targeted therapies. However the subsequent rebound in the pulse dose group and the trend toward increasing K^{ps} observed in the daily dose group are unlike findings from studies evaluating VEGF-targeted therapies. One possible explanation for these trends follows from considering the potential effects of dose and timing in the present study. The trend toward a reduction in K^{ps} measured in the pulsed dose group was observed

directly following two high-dose pulses of gefitinib. It is plausible that high-dose pulses of gefitinib might induce a trend toward reduction in microvessel leakiness over a transient window. It should be noted that a trend toward a slight reduction in K^{ps} was also observed in the control group and there was no statistical significance between or within groups. Future studies with larger sample sizes will be necessary to thoroughly investigate these trends.

Gefitinib-treated groups were not statistically distinguishable from the control group by mean tumor fPV. Observed trends revealed an increase in both gefitinib treatment groups between baseline and day 4, with the pulsed dose group showing a decrease afterwards. Such increases in mean tumor fPV are unlike trends observed in studies evaluating VEGF-targeted therapies where mean tumor fPV decreased or remained unchanged (36,37,40). Although these trends were not statistically significant, it is possible that HER TKIs as a class of inhibitors possess vascular characteristics that are distinct from VEGF-targeted therapies. One explanation for fPV increases following antiangiogenic therapy is a shift to larger vessels to compensate for the pruning of smaller leakier vessels (41). We previously reported improved vascular architecture—measured by anti-CD31 stains—from gefitinib administration (32).

In conclusion, although these findings are limited by the scope, design, and a small sample size in the present study, we show that the MRI parameters ADC, K^{ps}, fPV, and MRI-measured tumor volume are potentially sensitive to gefitinib induced changes in a human breast xenograft model. Changes detected by ADC measurements and DCE-MRI represent different physiological mechanisms and may thus provide complementary information on the timing and nature of the effects of different gefitinib treatment strategies on tumors. These results support further exploration of these MRI measures as noninvasive biomarkers of HER TKI-induced treatment effects.

Acknowledgments

The authors thank David Newitt, PhD, for providing the software used to fit T_1 maps and Julio Carballido-Gamio, PhD, for providing the software used for necrotic tissue segmentation.

Contract grant sponsor: National Institutes of Health (NIH); Contract grant number: R01 CA059487

References

1. Yarden Y. The EGFR family and its ligands in human cancer. Signaling mechanisms and therapeutic opportunities. Eur J Cancer. 2001; 37(Suppl 4):3–8. [PubMed: 11342194]
2. Rose-Hellekant TA, Sandgren EP. Transforming growth factor alpha- and c-myc-induced mammary carcinogenesis in transgenic mice. Nature. 2000; 19:1092–1096.
3. Ellis LM. Epidermal growth factor receptor in tumor angiogenesis. Hematol Oncol Clin North Am. 2004; 18:1007–1021. [PubMed: 15474332]
4. Kumar R, Yarmand-Bagheri R. The role of HER2 in angiogenesis. Semin Oncol. 2001; 28(5 Suppl 16):27–32. [PubMed: 11706393]
5. Moasser MM, Basso A, Averbuch SD, Rosen N. The tyrosine kinase inhibitor ZD1839 (“Iressa”) inhibits HER2-driven signaling and suppresses the growth of HER2-overexpressing tumor cells. Cancer Res. 2001; 61:7184–7188. [PubMed: 11585753]
6. Moulder S, Yakes F, Muthuswamy S, Bianco R, Simpson J, Arteaga C. Epidermal growth factor receptor (HER1) tyrosine kinase inhibitor ZD1839 (Iressa) inhibits HER2/neu (erbB2)-

overexpressing breast cancer cells in vitro and in vivo. Cancer Res. 2001; 61:8887–8895. [PubMed: 11751413]

7. Ciardiello F, Caputo R, Bianco R, et al. Antitumor effect and potentiation of cytotoxic drugs activity in human cancer cells by ZD-1839 (Iressa), an epidermal growth factor receptor-selective tyrosine kinase inhibitor. Clin Cancer Res. 2000; 6:2053–2063. [PubMed: 10815932]
8. Sirotnak FM, Zakowski MF, Miller VA, Scher HI, Kris MG. Efficacy of cytotoxic agents against human tumor xenografts is markedly enhanced by coadministration of ZD1839 (Iressa), an inhibitor of EGFR tyrosine kinase. Clin Cancer Res. 2000; 6:4885–4892. [PubMed: 11156248]
9. Sergina NV, Rausch M, Wang D, et al. Escape from HER-family tyrosine kinase inhibitor therapy by the kinase-inactive HER3. Nature. 2007; 445:437–441. [PubMed: 17206155]
10. Turetschek K, Preda A, Floyd E, et al. MRI monitoring of tumor response following angiogenesis inhibition in an experimental human breast cancer model. Eur J Nucl Med Mol Imaging. 2003; 30:448–455. [PubMed: 12722742]
11. Neil JJ. Measurement of water motion (apparent diffusion) in biological systems. Concepts Magn Reson. 1997; 9:385–401.
12. Gupta RK, Cloughesy TF, Sinha U, et al. Relationships between choline magnetic resonance spectroscopy, apparent diffusion coefficient and quantitative histopathology in human glioma. J Neurooncol. 2000; 50:215–226. [PubMed: 11263501]
13. Gupta RK, Sinha U, Cloughesy TF, Alger JR. Inverse correlation between choline magnetic resonance spectroscopy signal intensity and the apparent diffusion coefficient in human glioma. Magn Reson Med. 1999; 41:2–7. [PubMed: 10025604]
14. Pickles MD, Gibbs P, Lowry M, Turnbull LW. Diffusion changes precede size reduction in neoadjuvant treatment of breast cancer. Magn Reson Med. 2006; 24:843–847.
15. Yankeelov TE, Lepage M, Chakravarthy A, et al. Integration of quantitative DCE-MRI and ADC mapping to monitor treatment response in human breast cancer: initial results. Magn Reson Imaging. 2007; 25:1–13. [PubMed: 17222711]
16. Galons JP, Altbach MI, Paine-Murrieta GD, Taylor CW, Gillies RJ. Early increases in breast tumor xenograft water mobility in response to paclitaxel therapy detected by non-invasive diffusion magnetic resonance imaging. Neoplasia. 1999; 1:113–117. [PubMed: 10933044]
17. Rubesova E, Grell AS, Maertelaer VD, Metens T, Chao SL, Lemort M. Quantitative diffusion imaging in breast cancer: a clinical prospective study. J Magn Reson Imaging. 2006; 24:319–324. [PubMed: 16786565]
18. Guo Y, Cai Y, Cai Z, et al. Differentiation of clinically benign and malignant breast lesions using diffusion-weighted imaging. J Magn Reson Imaging. 2002; 16:172–178. [PubMed: 12203765]
19. Kuroki Y, Nasu K, Kuroki S, et al. Diffusion-weighted imaging of breast cancer with the sensitivity encoding technique: analysis of the apparent diffusion coefficient value. Magn Reson Med Sci. 2004; 3:79–85. [PubMed: 16093623]
20. Woodhams R, Matsunaga K, Iwabuchi K, et al. Diffusion-weighted imaging of malignant breast tumors: the usefulness of apparent diffusion coefficient (ADC) value and ADC map for the detection of malignant breast tumors and evaluation of cancer extension. J Comput Assist Tomogr. 2005; 29:644–649. [PubMed: 16163035]
21. Padhani AR. MRI for assessing antivascular cancer treatments. Br J Radiol. 2003; 76:S60–80. [PubMed: 15456715]
22. Knopp MV, Weiss E, Sinn HP, et al. Pathophysiologic basis of contrast enhancement in breast tumors. J Magn Reson Imaging. 1999; 10:260–266. [PubMed: 10508285]
23. Su MY, Wang Z, Nalcioglu O. Investigation of longitudinal vascular changes in control and chemotherapy-treated tumors to serve as therapeutic efficacy predictors. J Magn Reson Imaging. 1999; 9:128–137. [PubMed: 10030660]
24. Taylor JS, Tofts PS, Port R, et al. MR imaging of tumor microcirculation: Promise for the new millennium. J Magn Reson Imaging. 1999; 10:903–907. [PubMed: 10581502]
25. Turetschek K, Preda A, Novikov V, et al. Tumor microvascular changes in antiangiogenic treatment: assessment by magnetic resonance contrast media of different molecular weights. J Magn Reson Imaging. 2004; 20:138–144. [PubMed: 15221819]

26. Partridge SC, McKinnon GC, Henry RG, Hylton NM. Menstrual cycle variation of apparent diffusion coefficients measured in the normal breast using MRI. J Magn Reson Imaging. 2001; 14:433–438. [PubMed: 11599068]
27. Bezdek, JC. Pattern recognition with fuzzy objective function algorithm. New York: Plenum; 1981.
28. Klifa, C.; Carballido-Gamio, J.; Wilmes, L., et al. Quantification of breast tissue index from MR data using fuzzy clustering. San Francisco: IEEE; 2004.
29. Patlak CS, Blasberg RG, Fenstermacher JD. Graphical evaluation of blood-to-brain transfer constants from multiple-time uptake data. J Cereb Blood Flow Metab. 1983; 3:1–7. [PubMed: 6822610]
30. Tofts PS, Kermode AG. Measurement of the blood–brain barrier permeability and leakage space using dynamic MR imaging. Magn Reson Med. 1991; 17:357–367. [PubMed: 2062210]
31. Daldrup H, Shames DM, Wendland M, et al. Correlation of dynamic contrast-enhanced magnetic resonance imaging with histologic tumor grade: comparison of macromolecular and small-molecular contrast media. Pediatr Radiol. 1998; 28:67–78. [PubMed: 9472047]
32. Moasser M, Wilmes L, Wong C, et al. Improved tumor vascular function following high dose epidermal growth factor receptor tyrosine kinase inhibitor therapy. J Magn Reson Imaging. 2007; 26:1618–1625. [PubMed: 17968965]
33. Solit DB, She Y, Lobo J, et al. Pulsatile administration of the epidermal growth factor receptor inhibitor gefitinib is significantly more effective than continuous dosing for sensitizing tumors to paclitaxel. Clin Cancer Res. 2005; 11:1983–1989. [PubMed: 15756024]
34. Lyng H, Haraldseth O, Rofstad EK. Measurement of cell density and necrotic fraction in human melanoma xenografts by diffusion weighted magnetic resonance imaging. Magn Reson Med. 2000; 43:828–836. [PubMed: 10861877]
35. Checkley D, Tessier JJ, Kendrew J, Waterton JC, Wedge SR. Use of dynamic contrast-enhanced MRI to evaluate acute treatment with ZD6474, a VEGF signalling inhibitor, in PC-3 prostate tumours. Br J Cancer. 2003; 89:1889–1895. [PubMed: 14612898]
36. Li KL, Wilmes LJ, Henry RG, et al. Heterogeneity in the angiogenic response of a BT474 human breast cancer to a novel vascular endothelial growth factor-receptor tyrosine kinase inhibitor: assessment by voxel analysis of dynamic contrast-enhanced MRI. J Magn Reson Imaging. 2005; 22:511–519. [PubMed: 16161072]
37. Marzola P, Degrassi A, Calderan L, et al. Early antiangiogenic activity of SU11248 evaluated in vivo by dynamic contrast-enhanced magnetic resonance imaging in an experimental model of colon carcinoma. Clin Cancer Res. 2005; 11:5827–5832. [PubMed: 16115922]
38. Pham CD, Roberts TL, Bruggen Nv, et al. Magnetic resonance imaging detects suppression of tumor vascular permeability after administration of antibody to vascular endothelial growth factor. Cancer Invest. 1998; 16:225–230. [PubMed: 9589031]
39. Viloria-Petit A, Crombet T, Jothy S, et al. Acquired resistance to the antitumor effect of epidermal growth factor receptor-blocking antibodies in vivo: a role for altered tumor angiogenesis. Cancer Res. 2001; 61:5090–5101. [PubMed: 11431346]
40. Pradel C, Siauve N, Bruneteau G, et al. Reduced capillary perfusion and permeability in human tumour xenografts treated with the VEGF signalling inhibitor ZD4190: an in vivo assessment using dynamic MR imaging and macromolecular contrast media. Magn Reson Imaging. 2003; 21:845–851. [PubMed: 14599534]
41. Drevs J, Müller-Driver R, Wittig C, et al. PTK787/ZK 222584, a specific vascular endothelial growth factor-receptor tyrosine kinase inhibitor, affects the anatomy of the tumor vascular bed and the functional vascular properties as detected by dynamic enhanced magnetic resonance imaging. Cancer Res. 2002; 62:4015–4022. [PubMed: 12124335]

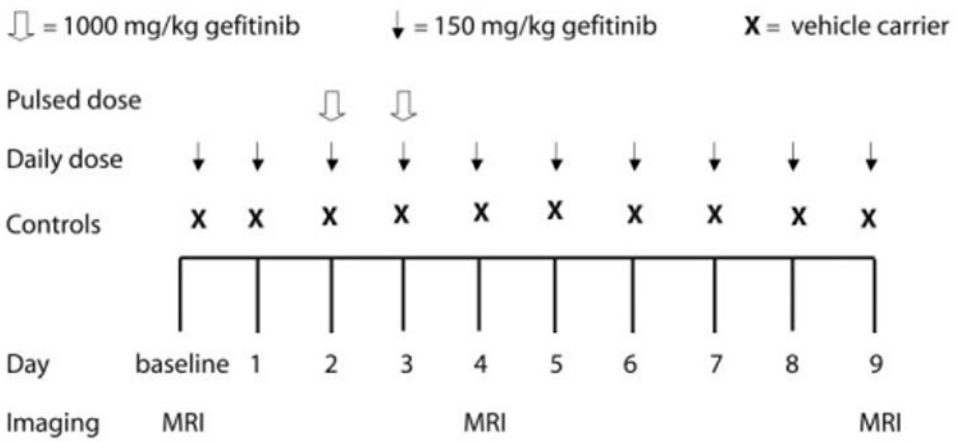

Figure 1.

Gefitinib treatment study schema. Mice in the gefitinib treatment study were treated according to three arms: daily dose (n = 6), pulsed dose (n = 6), and controls (n = 5). Mice in the daily dose treatment arm received gefitinib daily at the maximum tolerated daily dose of 150 mg/kg for 10 days. Mice in the pulsed dose treatment arm received two doses (day 2 and 3) of gefitinib at the maximum tolerated dose of 1000 mg/kg. Control mice were treated daily with vehicle carrier for 10 days. All mice were imaged at baseline, day 4, and day 9.

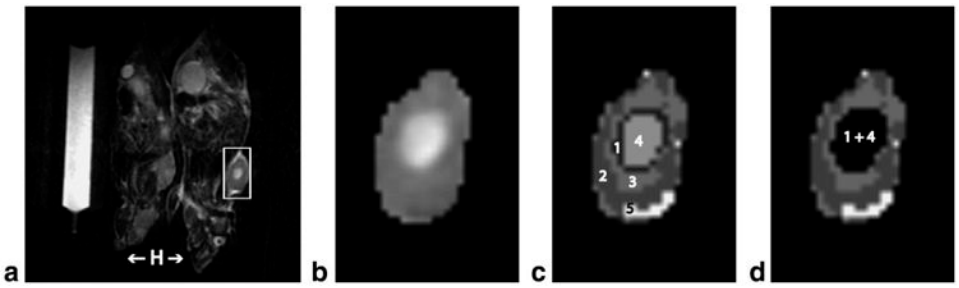

Figure 2.

Tumor necrosis segmentation. **a:** A representative T_2-weighted image of a pair of mice. Mice head (H) are indicated with arrows for orientation. Regions of interest (ROIs) were manually drawn around tumor margins on all tumor-appearing slices. The inset box demonstrates the extent of the tumor prior to ROI delineation. **b:** The tumor after isolation by ROI delineation. A region of central necrosis is evident. **c:** Pixel intensities from within the isolated tumor and with the number of clusters to be imposed served as input to the clustering algorithm. The clustering algorithm assigned pixels to clusters to minimize intra-cluster variance and generated clusters numbered 1 through 5. **d:** Generated clusters were visually inspected against the T_2-weighted image and categorized as potentially necrotic or not. Potentially necrotic clusters were then classified as truly necrotic if pixel intensities were beyond three standard deviations from mean tumor T_2-weighted intensity. Pixels belonging to necrotic clusters (clusters 1 and 4 in this case) were excluded from ADC analysis.

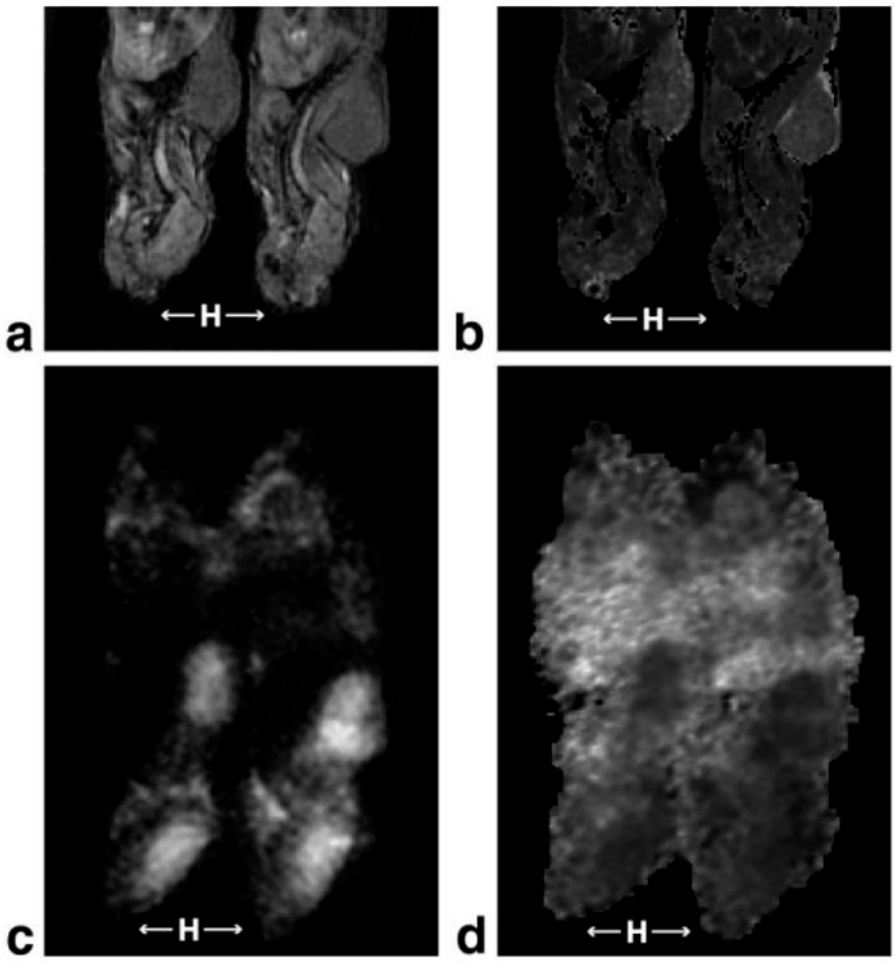

Figure 3.

Representative MR images. **a:** A representative T_1-weighted image for a pair of mice acquired at flip angle 40°. Mice head (H) are indicated with arrows for orientation. **b:** The corresponding T_1 map generated from T_1-weighted images acquired at flip angles of 40°, 20°, and 8°. **c:** A representative diffusion-weighted image (*b*-value = 603 s/mm^2). Mice head (H) are indicated with arrows for orientation. **d:** The corresponding ADC map.

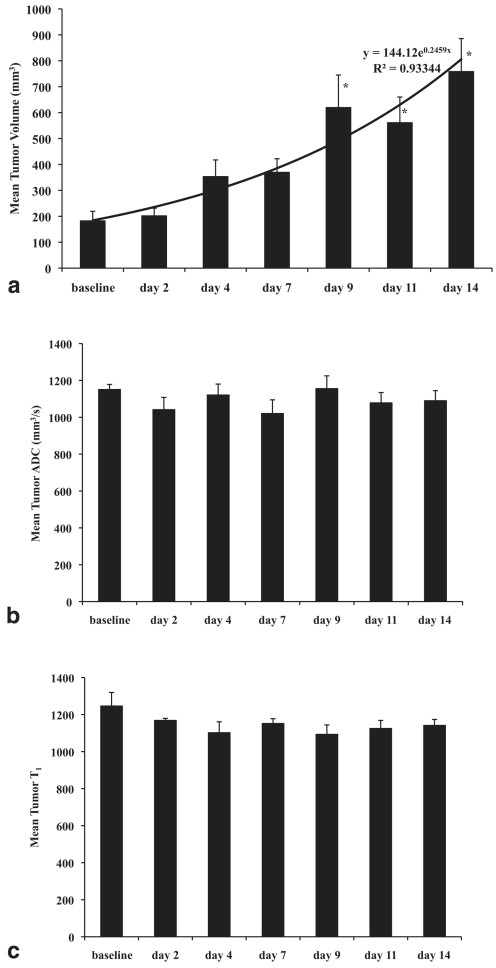

Figure 4.

Natural history study results. **a:** Mean tumor volume increased exponentially in untreated mice over the course of 14 days. Tumor volumes at later timepoints (day 9, day 11, day 14) were significantly different from tumor volumes at baseline. **b:** Mean tumor ADC values remained relatively uniform over the course of 14 days. **c:** Mean tumor T_1 values stabilized after a slight decrease from baseline to day 2. Error bars denote standard error. Asterisks denote statistical difference from baseline.

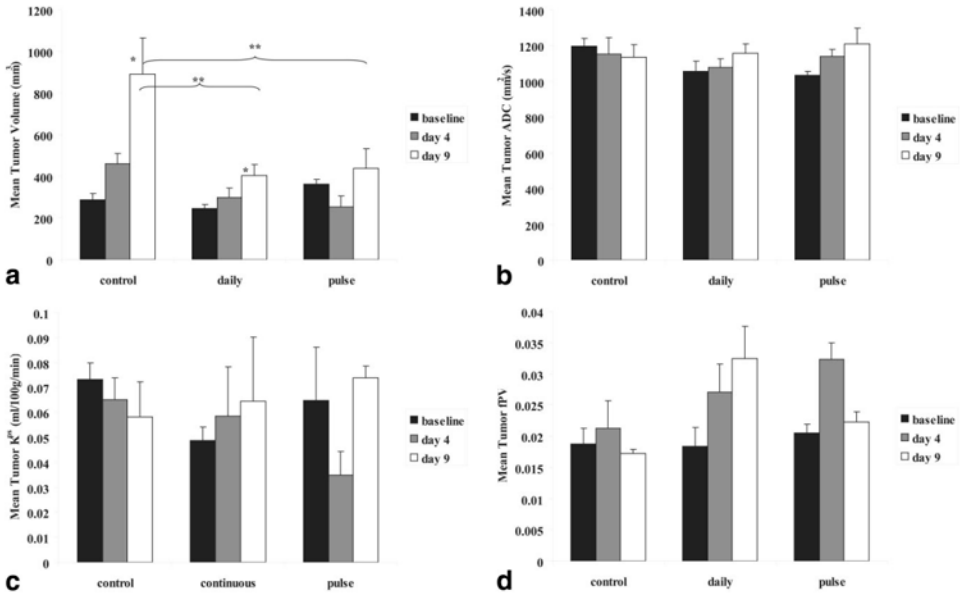

Figure 5.

Gefitinib treatment study results. **a:** Gefitinib treatment resulted in significant tumor growth inhibition; both gefitinib treated groups were statistically different from controls at day 9. A small reduction in tumor volume is observed with pulsed treatment at day 4. The gefitinib-treated groups were not statistically different from each other. **b:** There was a trend of increasing ADC in both gefitinib-treated groups while ADC in controls decrease slightly. **c:** Mean tumor K^{ps} decreased with pulsed treatment but rebounded afterwards and increased with daily treatment. **d:** Mean tumor fPV increased in both gefitinib treated groups, decreasing afterwards with pulsed treatment. Error bars denote standard error, single asterisks denote statistical difference from baseline within groups, while double asterisks denote statistical difference between groups at timepoints conjoined with braces.

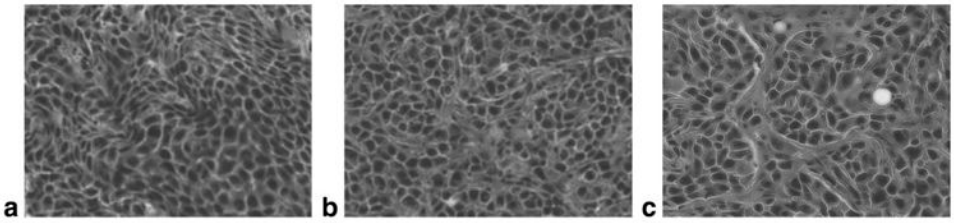

Figure 6.

H&E stains in the gefitinib treatment study (400×). Representative H&E stains of harvested tumor tissue for all three groups in the gefitinib treatment study are displayed at original magnification 400×: **(a)** control group, **(b)** daily treatment group, **(c)** pulsed treatment group. Gefitinib treatment resulted in significantly lower cell density in the treated groups but the treated groups were not significantly different from each other. Table 1 lists quantitative differences between the groups. Greater internuclear space was observed in the gefitinib-treated groups.

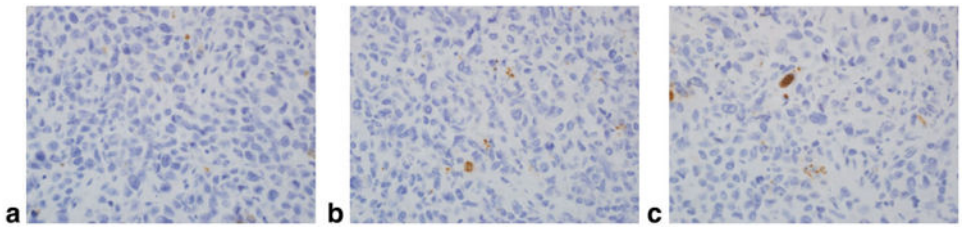

Figure 7.

Caspase-3 stains in the gefitinib treatment study (400×). Representative anticleaved capsase-3 stains of harvested tumor tissue for all three groups in the gefitinib treatment study are displayed at original magnification 400×: **(a)** control group, **(b)** daily treatment group, **(c)** pulsed treatment group. Minimal apoptotic activity was detected in all three groups but no significant differences were detected between any groups. Table 1 lists quantitative differences between groups.

Table 1

Histology and Immunohistochemistry

Groups	Cell density index[a]	Significance[b]	Apoptotic index[c]	Significance[b]
Controls	0.242 ± 0.014		0.0341 ±0.003	
Daily dose	0.166 ± 0.009	$P < 0.050$	0.0344 ± 0.004	$P > 0.050$
Pulsed dose	0.145 ± 0.008	$P < 0.050$	0.0321 ± 0.004	$P > 0.050$

[a] A cell density index derived from H&E slides as the ratio of the area occupied by cells in a given field to the total field area, revealed that both gefitinib treatment groups were significantly less dense than the control group. Means and standard error are provided for each group in the gefitinib treatment study.

[b] *P*-values reflect difference from controls.

[c] An apoptotic index derived from caspase-3-stained slides as the ratio of apoptosis stained cells in a given field to the total number of cells in the field, revealed no significant differences in apoptosis between groups in the gefitinib treatment study.